ELSEVIER

Chemical Engineering Science 61 (2006) 4451–4461

Chemical Engineering Science

www.elsevier.com/locate/ces

# Fluid motion around and through a porous cylinder

S. Bhattacharyya[a], S. Dhinakaran[a], A. Khalili[b,c,*]

[a]*Department of Mathematics, Indian Institute of Technology Kharagpur, Kharagpur, West Bengal 721302, India*
[b]*Max Planck Institute for Marine Microbiology, 28359 Bremen, Germany*
[c]*International University Bremen, 28759 Bremen, Germany*

Received 1 December 2005; received in revised form 3 February 2006; accepted 4 February 2006
Available online 23 February 2006

**Abstract**

The flow-field and solute transport through and around a porous cylinder is investigated numerically. The range of Reynolds number (based on the cylinder diameter and the uniform sinking rate of the cylinder) considered here is between 1 and 40 with Darcy number (*Da*) in the range $10^{-6} \leqslant Da \leqslant 1.5$ and porosity in the range $0.629 \leqslant \varepsilon \leqslant 0.999$. The motivation of the present study is the application of flow through porous cylinder extensively applied in nuclear biological chemical filters as well as reduction of carbon fines in filtered water. The influence of *Da* on the drag coefficient, separation angle, recirculation length, streamline and vorticity pattern are investigated. The drag ratio, defined as the ratio of drag coefficient of porous cylinder to that of solid cylinder, is found to approach zero from unity as *Da* is increased from $10^{-6}$ to 1.5. The separation point shifts towards the rear stagnation point as *Da* is increased. The time evolution of the solutal field at different Reynolds number and Darcy number is presented. A long slender concentration plume is found to evolve from the cylinder with decreasing concentration at the outer edge.


*Keywords:* Porous filter; Marine aggregates; Drag; Brinkman model; Mass transfer; Diffusion

## 1. Introduction

When a unidirectional flow encounters a porous cylinder, a complex flow field develops partially through and partially around the cylinder. The prediction of the flow rate passing through and flowing around the cylinder is not straight forward and depends on many factors such as the physical properties of the medium in question.

These flows occur in many practical applications and are important in different environmental issues. A closely related application is in the design of the nuclear biological chemical (NBC) filters allowing flow through a porous cylinder. NBC—filters are extensively used for the chemical, pharmaceutical and medical industries, where protection from dust/particle exposure is critical.

A direct link to flow through porous cylinder is given in a gas-cooled nuclear reactor where the nuclear fuel is separated from the rapidly circulating coolant by a porous graphite septum with a narrow gap between fuel and septum (Somasundaram and Mysels, 1975).

Apart from this, there are a series of related problems with different geometries such as seepage from streams bounded by porous banks, problems of leakage into aquifers and the displacement of oil from sandstones by shalewater influx and, recently in microbiology of marine aggregates (Kiorboe and Thygesen, 2001; Kiorboe et al., 2001). The flow relative to aggregates composed of small particles has relevance in several other practical situations, such as, the motion of clusters of materials in gas–solid reactors, the settling of dendritic structures in a molten metal and clusters in fluidized bed. The study of mobility and diffusivity of porous aggregates is also important in aerosol technology (Vainshtein et al., 2004).

A recent important application of flow through a porous cylinder is the use of this system in producing radial flow carbon (RFC) filters in the industry. The RFC cartridges are porous cylindrical rings of porous polyethylene applied for reducing of carbon fines in filtered water.

* Corresponding author. Max Planck Institute for Marine Microbiology, 28359 Bremen, Germany. Tel.: +49 4212028636; fax: +49 4212028690.
*E-mail addresses:* somnath@maths.iitkgp.ernet.in (S. Bhattacharyya), akhalili@mpi-bremen.de (A. Khalili).

0009-2509/$ - see front matter © 2006 Elsevier Ltd. All rights reserved.
doi:10.1016/j.ces.2006.02.012

After pioneering work of Baicorov (Von Wolfersdorf and Mönch, 2000), Von Wolfersdorf investigated the steady potential flow past a circular cylinder with porous surface (Von Wolfersdorf, 1988). Later, Heier and Von Wolfersdorf (1990) evaluated the solutions obtained before numerically (Heier and Von Wolfersdorf, 1990).

Recently, Von Wolfersdorf and Mönch (2000) have studied the potential flow past a porous circular cylinder. When taking the Darcy equation for description of the flow inside the porous cylinder, the complete flow domain could be formulated as a nonlinear boundary-value problem of Poincarė type.

The problem of flow and concentration distribution around and through a porous cylinder for low and moderate Reynolds number range for non-potential flows does not exist in the literature. This is exactly the focus of the present work.

Several authors have studied the flow past an isolated porous cylinder or sphere namely, Masliyah and Polikar (1980), Nandakumar and Masliyah (1982), Adler (1992), Noymer et al. (1998), Vanni (2000) and Vainshtein et al. (2002, 2004). In most of those studies the flow field inside the porous bodies is described by the Darcy equation and the Navier–Stokes equations usually under creeping flow conditions to model the flow outside the body. This approach requires an appropriate boundary condition at the interface of the porous body. However, in many applications non-Darcian effects including shear and non-linear effects within the porous matrix and the viscous effects at the interface becomes significant under various conditions. Hence, for the extension of Darcy equation, the Brinkman and Forchheimer term are used.

As the solution technique, a single-domain approach is used which consider the porous layer as a pseudo-fluid and the composite region as a continuum. This leads to a single momentum equation, namely, a modified Navier–Stokes equation with an additional Darcy and, eventually, Forchheimer term. The adequate expression of the momentum equation for the fluid or for the porous medium is retained through the corresponding value of the permeability. This formulation has been widely used by several authors (e.g., Beckermann and Viskanta, 1988; Vafai and Kim, 1989; Basu and Khalili, 1999), since it does not require any explicit boundary condition at the fluid–porous interface. In single-domain approach the values from both sides of the interface is used to obtain solutions, and therefore matching of variable values is inherent in the formulation itself. Thus, the single-domain approach is doing away with the need for separate interface conditions. We investigated the Reynolds number range of up to 40, the Darcy number range of $10^{-2}$–$10^{-6}$ and the porosity range of 0.993–0.629. The range studied below is chosen also having in mind a marine-related application for studying sinking porous aggregates. These aggregates sink at velocities up to 100 m or more per day, and are thus characterised by Reynolds number up to 20 and porosity above 0.9 (Alldredge and Gotschalk, 1988, 1989). Besides, the flow around a circular cylinder is steady for Reynolds number below 40 (Braza et al., 1986). The solute distribution in and around the porous cylinder is described by solving the diffusion–advection equation. The governing equation of the problem is presented in Section 2 followed by Section 3 on the numerical method used. The results and discussion are made in Section 4. In Section 5, we present the conclusion.

## 2. Governing equations

We consider a long cylinder of radius $a$ placed in a uniform flow (from left to right) with velocity $U$. A two-dimensional, laminar, incompressible and steady flow of a fluid with constant properties is considered. The single-domain approach (Basu and Khalili, 1999) is adopted in the present analysis.

The fluid velocity averaged to a volume containing fluid only ($V$) and the filter velocity ($v$) are related to each other by the Dupuit–Forchheimer equation (Nield and Bejan, 1998) by $v = \varepsilon.V$, where $\varepsilon$ is the porosity. We take the characteristic length as $a$ and characteristic velocity $U$ with center of the cylinder as the origin in polar co-ordinates $(r, \theta)$ and the initial line along the direction of the uniform stream. The single set of equations in non-dimensional form can be written as

$$\frac{1}{r}\frac{\partial(rv)}{\partial r} + \frac{1}{r}\frac{\partial u}{\partial \theta} = 0, \tag{1}$$

$$\begin{aligned}\frac{\partial u}{\partial t} + \frac{1}{\varepsilon}\left(\frac{u}{r}\frac{\partial u}{\partial \theta} + v\frac{\partial u}{\partial r} + \frac{uv}{r}\right) &= -\varepsilon\frac{1}{r}\frac{\partial p}{\partial \theta} + \Lambda\frac{2\varepsilon}{Re}\left(\frac{1}{r}\frac{\partial}{\partial r}\left(r\frac{\partial u}{\partial r}\right) + \frac{1}{r}\frac{\partial}{\partial \theta}\left(\frac{1}{r}\frac{\partial u}{\partial \theta}\right)\right.\\ &\quad \left. + \frac{2}{r^2}\frac{\partial v}{\partial \theta} - \frac{u}{r^2}\right) - B\frac{2\varepsilon}{ReDa}u\\ &\quad - \frac{1.75}{\sqrt{150}}\frac{1}{\sqrt{Da}}\frac{\sqrt{u^2+v^2}}{\sqrt{\varepsilon}}u,\end{aligned} \tag{2}$$

$$\begin{aligned}\frac{\partial v}{\partial t} + \frac{1}{\varepsilon}\left(\frac{u}{r}\frac{\partial v}{\partial \theta} + v\frac{\partial v}{\partial r} - \frac{u^2}{r}\right) &= -\varepsilon\frac{\partial p}{\partial r} + \Lambda\frac{2\varepsilon}{Re}\left(\frac{1}{r}\frac{\partial}{\partial r}\left(r\frac{\partial v}{\partial r}\right) + \frac{1}{r}\frac{\partial}{\partial \theta}\left(\frac{1}{r}\frac{\partial v}{\partial \theta}\right)\right.\\ &\quad \left. - \frac{2}{r^2}\frac{\partial u}{\partial \theta} - \frac{v}{r^2}\right) - B\frac{2\varepsilon}{ReDa}v\\ &\quad - \frac{1.75}{\sqrt{150}}\frac{1}{\sqrt{Da}}\frac{\sqrt{u^2+v^2}}{\sqrt{\varepsilon}}v.\end{aligned} \tag{3}$$

Here,

$$B = \text{Binary constant}\begin{cases}0 & \text{outside the porous cylinder,}\\ 1 & \text{inside the porous cylinder,}\end{cases}$$

$$\varepsilon = \text{Porosity}\begin{cases}1 & \text{outside the porous cylinder,}\\ 0<\varepsilon<1 & \text{inside the porous cylinder,}\end{cases}$$

$\Lambda = \bar{\mu}/\mu$ denotes the viscosity ratio; $Re = \rho U 2a/\mu$ is the Reynolds number and $Da = k/a^2$ is the Darcy number. In the fluid region $Da$ is assumed to take an infinitely large value.

The porosity ($\varepsilon$) and the Darcy number ($Da$) could be related through the Carman–Kozeny relation (Nield and Bejan, 1998)

$$k = \frac{1}{180}\frac{\varepsilon^3 d_p^2}{(1-\varepsilon)^2},$$

where $k$ is the permeability and $d_p$ is the characteristic diameter of a particle in the porous aggregate, each of which may be of

100 μm in diameter. The Forchheimer terms in the momentum equations are obtained based on Nithiarasu et al. (1997).

The dimensionless variables are defined as

$$\theta = \overline{\theta}, \quad r = \frac{\overline{r}}{a}, \quad t = \frac{\overline{t}U}{a}, \quad p = \frac{\overline{p}}{\rho U^2},$$

$$u = \frac{\overline{u}}{U}, \quad v = \frac{\overline{v}}{U}, \quad \phi = \frac{\overline{c}}{c_i},$$

where $u$ is the cross-radial velocity component, $v$ is the radial velocity component, $\phi$ is the dimensionless concentration, $c_i$ is the initial concentration within the porous cylinder, $\rho$ is the density, $p$ is the pressure and $t$ is the time. Here, the variables with bar denotes the dimensional variables.

The mass transport equation valid in both the fluid and the porous region is given by

$$\frac{\partial \phi}{\partial t} + \frac{1}{\varepsilon}\left(\frac{u}{r}\frac{\partial \phi}{\partial \theta} + v\frac{\partial \phi}{\partial r}\right) = \Gamma \frac{2}{ReSc}\left(\frac{\partial^2 \phi}{\partial r^2} + \frac{1}{r}\frac{\partial \phi}{\partial r} + \frac{1}{r^2}\frac{\partial^2 \phi}{\partial \theta^2}\right), \tag{4}$$

where $\Gamma = \overline{\sigma}/\sigma =$ diffusivity ratio, $Sc = \nu/\sigma =$ Schmidt number and $\overline{\sigma}$, $\sigma$ are the diffusivities of $\phi$ inside the porous and the fluid layers, respectively. The diffusivity ratio is taken as 1.0.

The governing equations (2)–(4) are subjected to the following initial and boundary conditions:

*Initial conditions* ($t = 0$):

$$u = U\sin\theta, \quad v = -U\cos\theta \quad \text{(everywhere)},$$

$$\phi = \begin{cases} 0 & \text{in fluid region,} \\ 1 & \text{in porous region.} \end{cases}$$

*Boundary conditions* ($t > 0$):

$$u = U\sin\theta, \quad v = -U\cos\theta, \quad \phi = 0 \quad \text{(upstream boundary)},$$

$$\frac{\partial u}{\partial r} = 0, \quad \frac{\partial v}{\partial r} = 0, \quad \frac{\partial \phi}{\partial r} = 0 \quad \text{(downstream boundary)}.$$

The coefficient of the drag on the cylinder is given by

$$C_D = \frac{\text{Drag force}}{0.5\rho U_\infty^2 2a},$$

$$C_D = C_{D_V} + C_{D_P},$$

where

$$C_{D_V} = \frac{2}{Re}\int_0^{2\pi} \omega_w \sin x \, dx, \quad C_{D_P} = \frac{2}{Re}\int_0^{2\pi} p_w \cos x \, dx,$$

where the subscripts $V$ and $P$ represent the contributions of the viscous and pressure forces, respectively. $p_w$ is the dimensionless wall pressure and $\omega_w$ is the dimensionless wall vorticity defined as $\omega_w = \omega a/U$. The wall pressure coefficient $C_P$ is obtained as

$$C_P = (\overline{p} - \overline{p}_o + \tfrac{1}{2}\rho U^2)/(\tfrac{1}{2}\rho U^2)$$

with $p_o$ the front stagnation point pressure.

## 3. Numerical method

The governing equations (1)–(4) are solved numerically using a finite volume method over a staggered grid system. In the staggered grid arrangement the velocity components are stored at the midpoints of the cell sides to which they are normal. The scalar quantities such as the pressure and concentration are stored at the center of the cell. The discretized forms of the governing equations are obtained by integrating over elemental rectangular cells using finite volume method.

We use a pressure correction-based iterative algorithm SIMPLE (Patankar, 1980) for solving the governing equations with those boundary conditions specified previously. A first-order implicit scheme is used for discretising the time derivatives. The pressure link between continuity and momentum is accomplished by transforming the continuity equation into a Poisson equation for pressure. The Poisson equation implements a pressure correction for a divergent velocity field. At each time step the resulting tridiagonal system of algebraic equations are solved through a block elimination method. A single iteration consists of sequential solution of

1. An implicit calculation of the $r$, $\theta$ momentum equation is performed.
2. The Poisson equation for pressure correction is solved using the successive under relaxation method. In this case the under-relaxation factor is chosen as 0.6.
3. The velocity field at each cell is updated using the pressure correction.

Iteration at each time step continues until the divergence-free velocity field is obtained. However, for this purpose the divergence in each cell is towed below a preassigned small quantity of $\leqslant 10^{-5}$. Using the updated value of the velocity, the mass transfer equation (4) is solved at each time step through central difference approximation to obtain $\phi$ at each cell center. A time-dependent numerical solution is achieved by advancing the flow field variables through a sequence of short time steps of duration $\delta t$ of 0.005. Further reduction of $\delta t$ does not produce any significant difference in drag coefficient ($\overline{C}_D$).

The parameters such as porosity ($\varepsilon$) and permeability ($Da$) usually undergo large changes at the interface between the fluid and the porous layer. In the single-domain approach this becomes a major source of numerical difficulty. The harmonic-mean formulation is used to handle the abrupt change in the above-mentioned parameters. As the velocity field vary more rapidly near the interface ($r = 1$) than elsewhere, a finer grid distribution is imposed around $r = 1$.

A series of test runs were made for determining the optimal grid size and the runs were performed with various grid sizes for two different lengths of the outer boundary ($L_d$). The outer boundary is chosen large enough that the influence of the boundary condition on the wall shear stress is negligible. The code was tested for four different grid sizes namely $300 \times 190$, $400 \times 241$, $440 \times 260$ and $460 \times 271$ with the first and second number being the number of mesh points in the radial and in the cross-radial direction. We considered a non-uniform grid

Table 1
Effect of mesh size and external boundary on $\overline{C}_D$ at $Re = 40$ and $Da = 10^{-6}$ ($\varepsilon = 0.629$)

| Case | Cell size ($\Delta\theta \times \Delta r$) | Outer boundary ($L_d$) | Co-efficient of drag ($\overline{C}_D$) | Grid size ($m \times n$) |
|---|---|---|---|---|
| 1. | 0.0209 × 0.025 | | 1.562 | 300 × 190 |
| 2. | 0.0157 × 0.010 | 20 | 1.594 | 400 × 241 |
| 3. | 0.0143 × 0.005 | | 1.604 | 440 × 260 |
| 4. | 0.0136 × 0.005 | | 1.608 | 460 × 271 |
| 5. | 0.0209 × 0.025 | | 1.545 | 300 × 224 |
| 6. | 0.0157 × 0.010 | 30 | 1.581 | 400 × 261 |
| 7. | 0.0143 × 0.005 | | 1.597 | 440 × 274 |
| 8. | 0.0136 × 0.005 | | 1.599 | 460 × 291 |

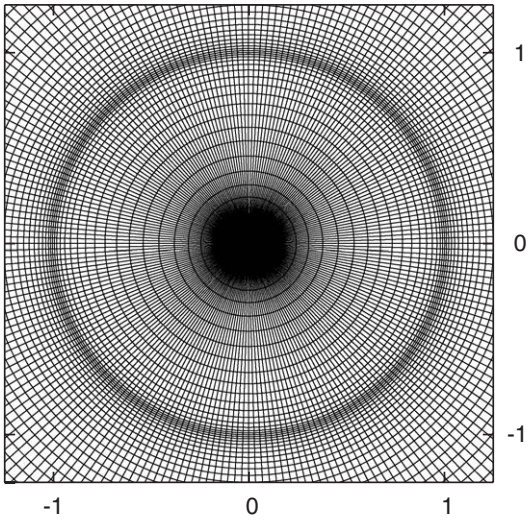


Fig. 1. Grid resolution in and around the cylinder interface at a grid size of 440 × 270.

distribution along the radial direction but a uniform grid is considered along the $\theta$-direction. Grids are stretched through an arithmetic progression. In the $r$-direction the distance of the first grid point from the cylinder surface varies between 0.025 to 0.005. We considered the variation of the outer radius $L_d$ between 20 and 30 times the radius of the cylinder. Table 1 shows the percentage difference on the drag coefficient ($\overline{C}_D$) at various grid sizes at different values of outer boundary ($L_d$). The grid sensitivity analysis is performed for $Re = 40$ and $Da = 10^{-6}$. The percentage difference in $\overline{C}_D$ between the two grids namely 440 × 260 and 460 × 271 at extent of the outer domain boundary $L_d = 20$ is 0.25%. Whereas, at $L_d = 30$, percentage difference in $\overline{C}_D$ between the two grids, 440 × 274 and 460 × 291 is 0.12%. The 440 × 260 grid at $L_d = 20$ and 440 × 274 grid at $L_d = 30$ captured the best flow field and the maximum percentage difference in $\overline{C}_D$ when these two grids sizes are used is 0.44%. Thus, our grid sensitivity study suggests that the grid-independent results could be achieved using a 440 × 260 grid at a outer boundary of 20, which took the least computational time. The grid resolution near the surface of the porous cylinder for 440 × 260 grid is shown in Fig. 1.

In order to check the accuracy of our method we have compared our results for the flow past a solid cylinder with those of

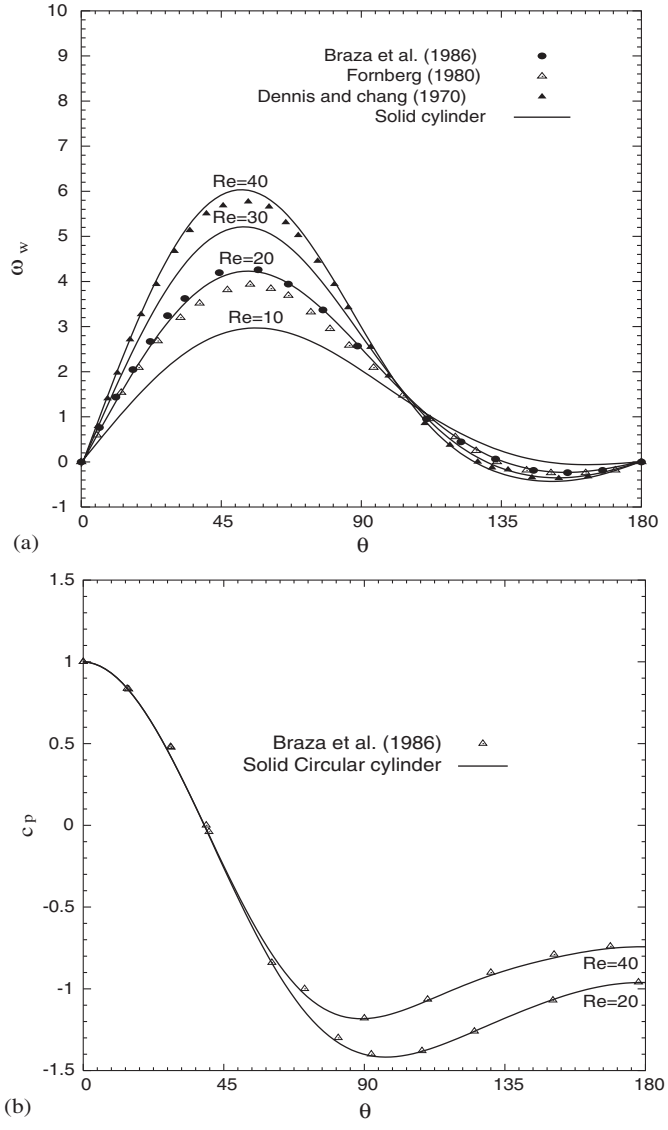


Fig. 2. (a) Comparison of wall vorticity and (b) comparison of wall pressure, for the flow past a solid circular cylinder.

Braza et al. (1986), Fornberg (1980), Dennis and Chang (1970) and Sucker and Brauer (1975). The dimensionless wall vorticity ($\omega_w$) and the computed wall pressure coefficient ($C_P$) is found to be in good agreement with those of Braza et al. (1986), Fornberg (1980) and Dennis and Chang (1970) (Figs. 2a, b).

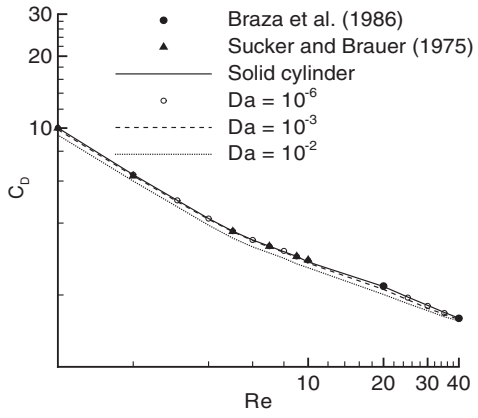


Fig. 3. Variation of drag coefficient at various $Re$ for $Da = 10^{-6}$ ($\varepsilon = 0.629$), $Da = 10^{-3}$ ($\varepsilon = 0.977$) and $Da = 10^{-2}$ ($\varepsilon = 0.993$).

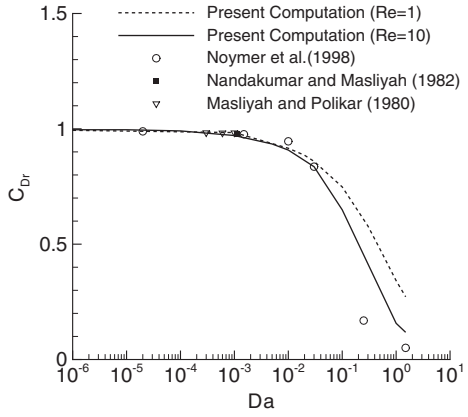


Fig. 4. Drag ratio at $Re = 1, 10$ as a function of $Da$.

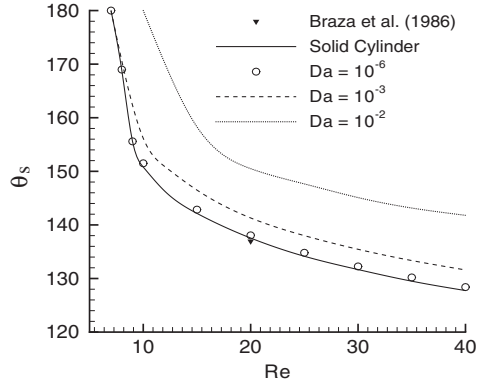


Fig. 5. Separation angle as a function of $Re$ at $Da = 10^{-6}$ ($\varepsilon = 0.629$), $Da = 10^{-3}$ ($\varepsilon = 0.977$) and $Da = 10^{-2}$ ($\varepsilon = 0.993$).

The computed drag-coefficient ($\overline{C}_D$) plotted as a function of Reynolds number compared with the numerical results of Braza et al. (1986) and empirical data determined by Sucker and Brauer (1975) is shown in Fig. 3. We see the excellent comparisons between the computational and empirical results. We have also compared our results for the drag ratio $\overline{C}_{Dr}$ (defined as the ratio of drag coefficient for the porous cylinder to that of solid cylinder), at different Darcy number and porosity

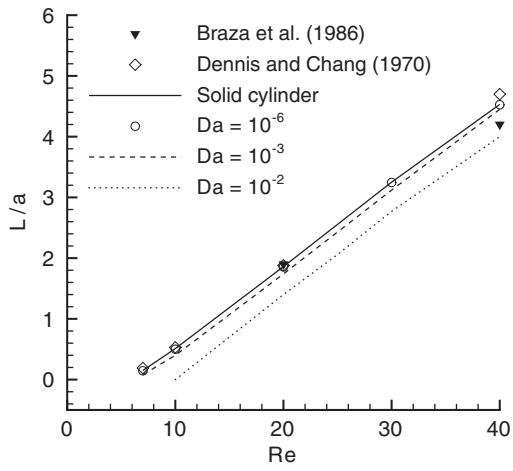


Fig. 6. Predicted wake-length as a function of $Re$ at $Da = 10^{-6}$ ($\varepsilon = 0.629$), $Da = 10^{-3}$ ($\varepsilon = 0.977$) and $Da = 10^{-2}$ ($\varepsilon = 0.993$).

at $Re = 10$ with results of Noymer et al. (1998), Masliyah et al. (1980) and Nandakumar et al. (1982) and found them in good agreement (Fig. 4). The angle ($\theta_s$) at which the external flow separates from the surface of the solid cylinder compared with Braza et al. (1986) is depicted in Fig. 5 as a function of Reynolds number. A good comparison is obtained with those of Braza et al. (1986) and Dennis and Chang (1970) for the length of the wake ($L/a$) formed behind the cylinder (Fig. 6).

## 4. Results and discussion

The present flow field is governed by four parameters namely, Reynolds number ($Re$), Schmidt number ($Sc$), Darcy number ($Da$) and porosity ($\varepsilon$). However, the Darcy number and porosity are related through the Carman–Kozeny relation. We have restricted our study for $Re$ up to 40 and $\varepsilon$ around 0.9. The flow field at different values of $Re$ and $Da$ is presented in Figs. 3–12, whereas the distribution of concentration inside and around the cylinder is presented in Figs. 13–15.

The variation of the drag coefficient ($\overline{C}_D$) of the porous cylinder at $Da = 10^{-2}$ with time is shown in Fig. 7 at different $Re$. The figure shows that flow field becomes steady after an initial transition within the range of Reynolds number considered.

The variation of drag coefficient as a function of Reynolds number ($1 \leqslant Re \leqslant 40$) is shown in Fig. 3 for $Da = 10^{-6}$, $10^{-3}$ and $10^{-2}$ in log-scale in both the axes. From the figure it is evident that the drag coefficient is nearly the same as that of solid cylinder for $Da = 10^{-6}$ for the range of Reynolds number considered in this investigation. Thus at $Da = 10^{-6}$ ($\varepsilon = 0.629$), even though the void volume is 62.9% of the total volume, the porous cylinder behaves like a impermeable cylinder. The drag coefficient at $Da = 10^{-3}$ and $10^{-2}$ are found to be less than the $Da = 10^{-6}$ case. At low Reynolds number ($Re \leqslant 5$) the percentage difference in $\overline{C}_D$ for $Da = 10^{-2}$ with that of solid cylinder is almost found to be independent of Reynolds number. For example, the percentage difference in drag coefficient at $Re = 1$ and 5 with that of solid cylinder at $Da = 10^{-2}$ is 7.13% and 7.10%, respectively. However, $\overline{C}_D$ reduces monotonically as $Re$

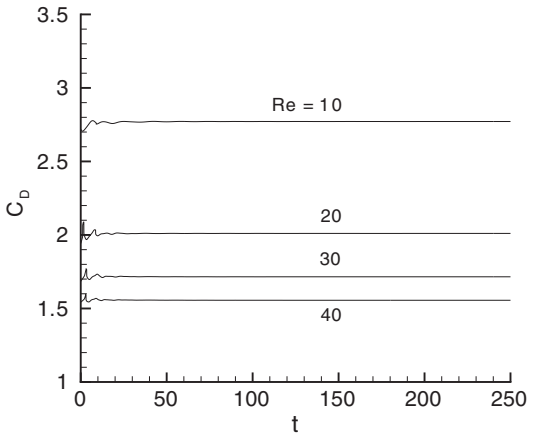


Fig. 7. Time evolution of drag coefficient for different $Re$ at $Da = 10^{-2}$ ($\varepsilon = 0.993$).

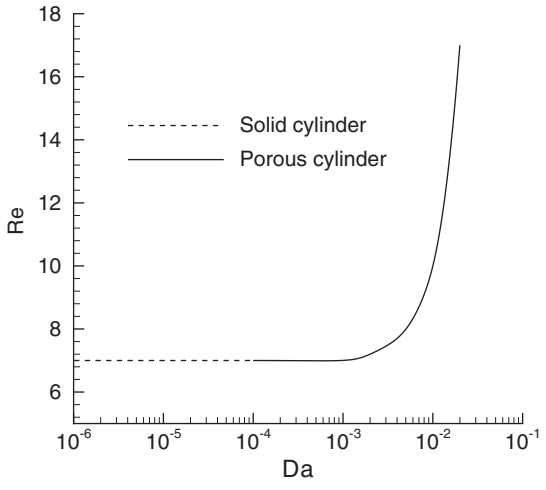


Fig. 8. Onset of flow separation at different $Da$.

increases from 5 to 40 for all values of $Da$ ($=10^{-2}, 10^{-3}, 10^{-6}$). For example, at $Re = 10$ the percentage difference of $\overline{C}_D$ at $Da = 10^{-3}$ and $10^{-2}$ with that of the solid cylinder is 2.57% and 5.89%, respectively. Whereas, at $Re = 40$ the difference reduced to 0.63% and 1.92%, respectively. It is to be noted that the inclusion of the Forchheimer term does not produce any significant change in drag coefficient.

Fig. 4 shows the effect of Darcy number on the drag ratio ($\overline{C}_{Dr}$) at $Re = 1$ (dashed line) and $Re = 10$ (solid line). From the figure it is seen that $\overline{C}_{Dr}$ is close to unity for $10^{-6} \leqslant Da \leqslant 10^{-4}$ and thereafter it approaches zero as the permeability ($Da$) is increased. A highly permeable cylinder allows the fluid to flow through it with the least resistance, hence the drag must approach zero for the high permeability case. Whereas, a porous cylinder with very low permeability will allow little or no fluid to pass through it. For $Da > 10^{-2}$ the drag ratio at $Re = 1$ is greater than the drag ratio at $Re = 10$. We have compared our results for the drag ratio with those of Noymer et al. (1998) at $Re = 10$ for various $Da$. Noymer et al. (1998) used the Darcy model to describe the flow through the porous cylinder. Our

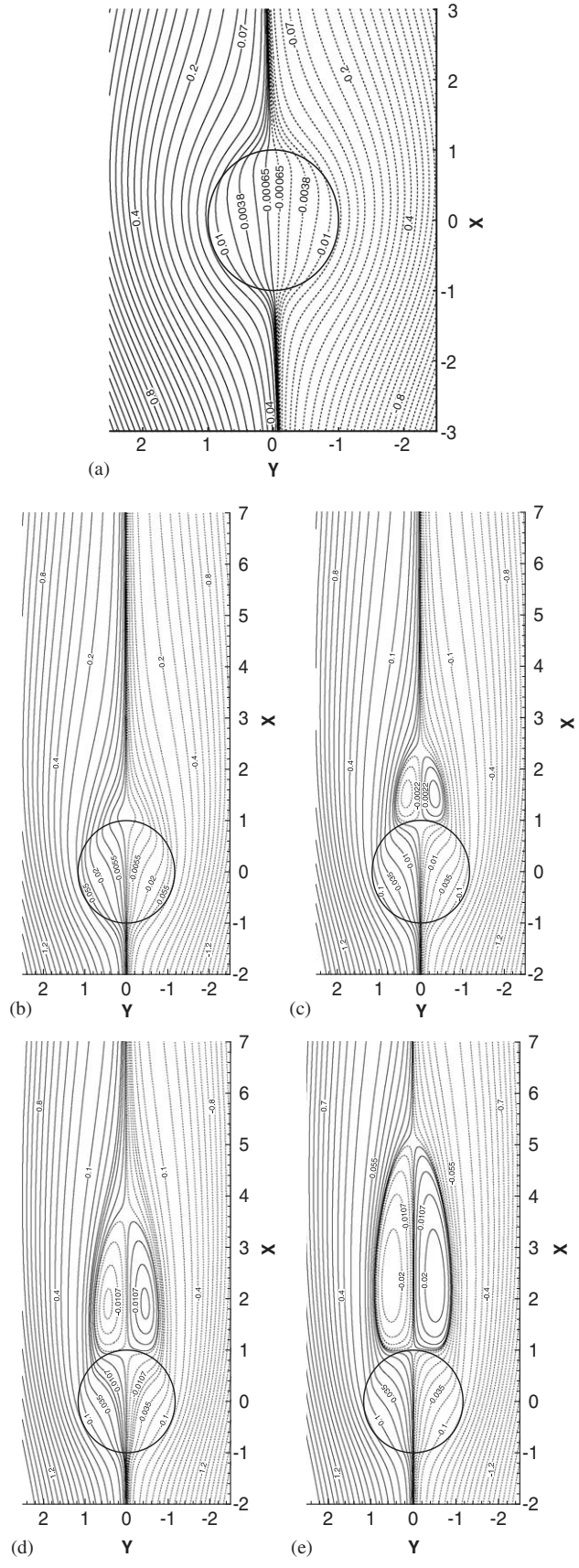


Fig. 9. Streamlines for the flow through the porous cylinder (solid and dashed lines refer to positive and negative values, respectively) at $Da = 10^{-2}$ ($\varepsilon = 0.993$) (a) $Re = 1$; (b) $Re = 10$; (c) $Re = 20$; (d) $Re = 30$ and (e) $Re = 40$.

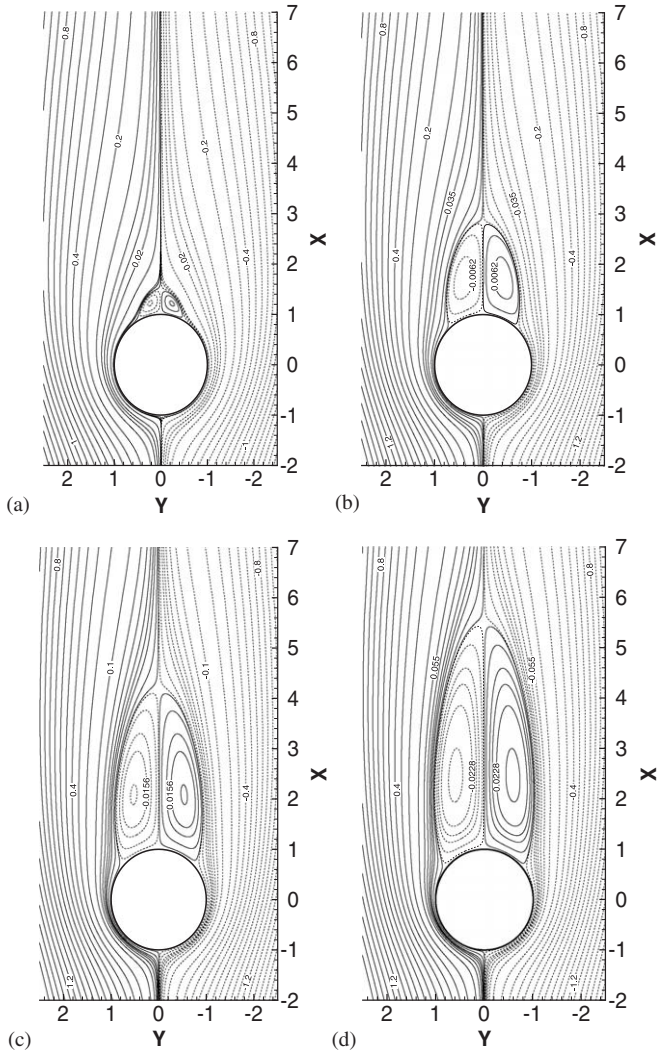


Fig. 10. Streamlines for the flow through the porous cylinder (solid and dashed lines refer to positive and negative values, respectively) at $Da = 10^{-6}$ ($\varepsilon = 0.629$) (a) $Re = 10$; (b) $Re = 20$; (c) $Re = 30$ and (d) $Re = 40$.

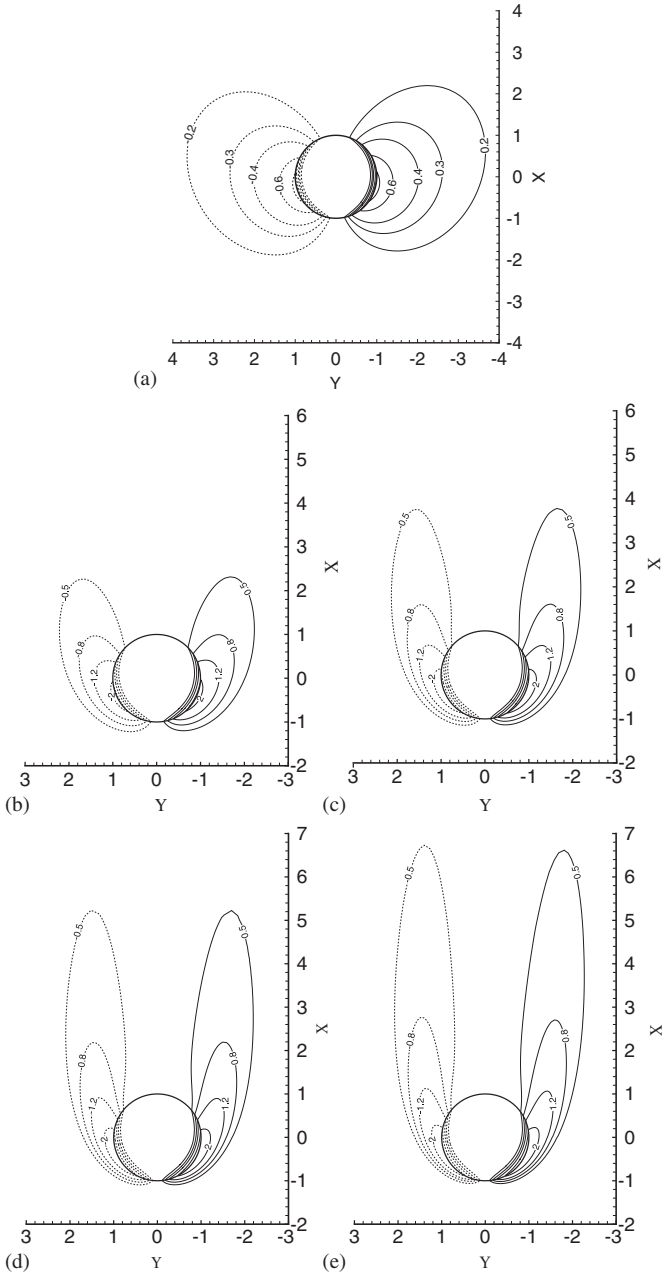


Fig. 11. Distribution of vorticity for the flow through the porous cylinder (solid and dashed lines refer to positive and negative values, respectively) at $Da = 10^{-2}$ ($\varepsilon = 0.993$) (a) $Re = 1$; (b) $Re = 10$; (c) $Re = 20$; (d) $Re = 30$ and (e) $Re = 40$.

results are in excellent agreement with them up to a $Da = 10^{-4}$. Beyond this, a deviation of our results from their result occurs. This is due to the reason that the value of $Da = 10^{-4}$ represents the limit where viscous effects are important and this becomes practically Darcian as $Da$ is further reduced (Jimenez-Islas et al., 1999).

The angle of flow separation from the cylinder ($\theta_s$) is presented in Fig. 5 for different values of Reynolds number and $Da = 10^{-6}$, $10^{-3}$, $10^{-2}$. The separation angle is measured from the front stagnation point. It is evident from the figure that the separation point shifts towards the rear stagnation point ($\theta = 180°$) as $Da$ increases. The external flow field will experience separation only if the inertial forces are of sufficient magnitude. A porous cylinder allows a finite fluid velocity at the interface, which becomes more important at higher $Da$. This velocity has the effect of reducing the relative importance of the inertial forces in the external field. Hence, separation is delayed with respect to Reynolds number compared to the solid cylinder case. The situation is similar to an injection from a porous cylinder (Mathelin et al., 2002). The separation angle varies almost linearly with Reynolds number when $Re$ is greater than 20 for porous as well as solid cylinder case.

The length of the symmetric wake formed behind the porous cylinder is found to vary with $Da$. The predicted wake length ($L/a$) is plotted as a function of Reynolds number in Fig. 6 for solid cylinder and porous cylinder at $Da = 10^{-6}$, $10^{-3}$ and $10^{-2}$ ($\varepsilon = 0.629$, 0.977 and 0.993). Our prediction shows that the wake length increases linearly with an increment in Reynolds number for both the solid and porous cylinder. We found a

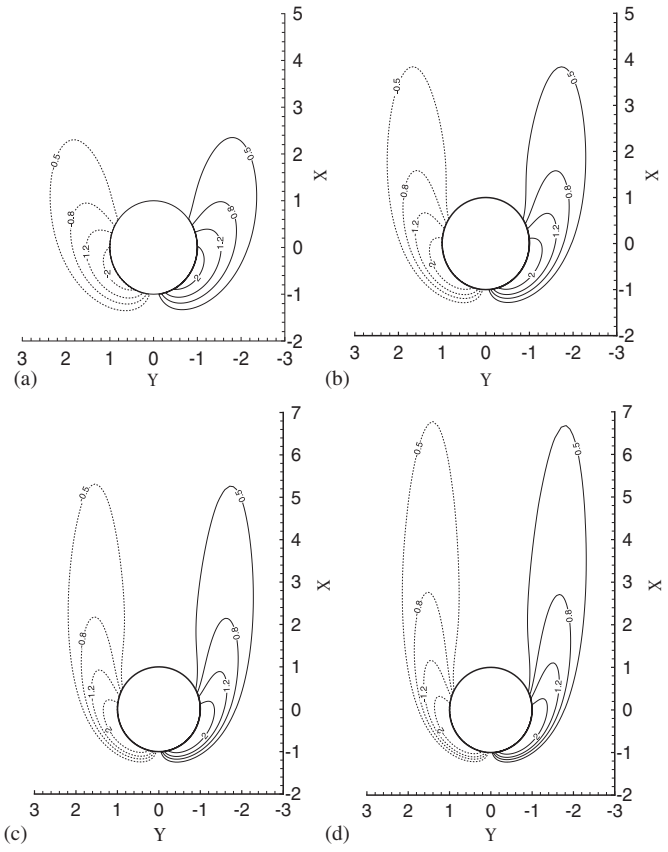


Fig. 12. Distribution of vorticity for the flow through the porous cylinder (solid and dashed lines refer to positive and negative values, respectively) at $Da = 10^{-6}$ ($\varepsilon = 0.629$) (a) $Re = 10$; (b) $Re = 20$; (c) $Re = 30$ and (d) $Re = 40$.

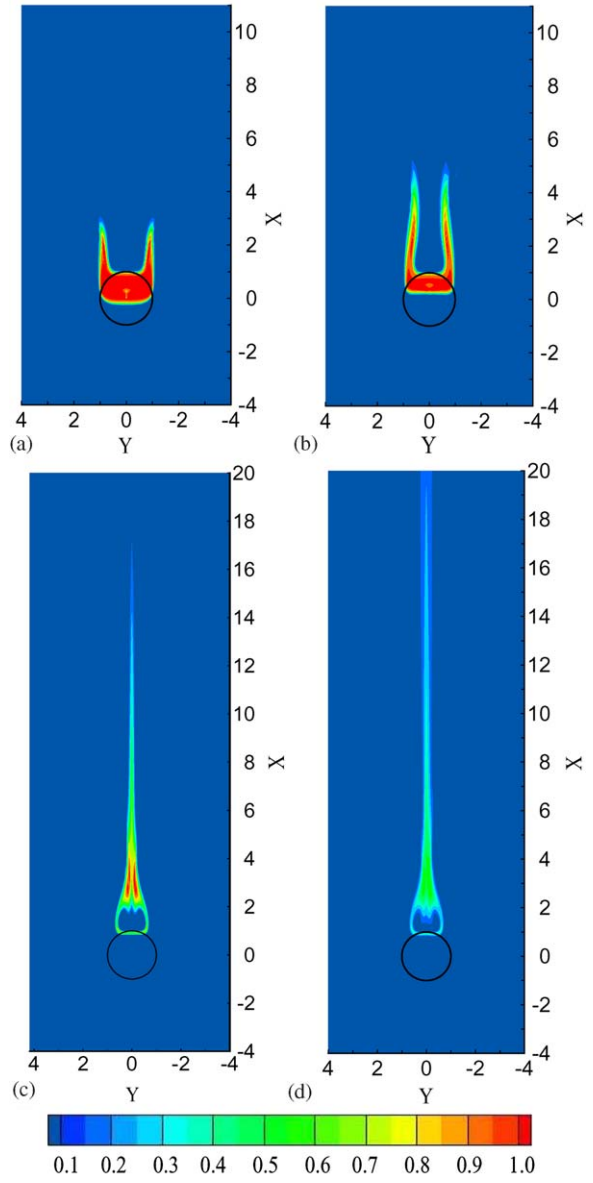


Fig. 13. Concentration field in and around the porous cylinder for $Re = 20$ and $Da = 10^{-2}$ ($\varepsilon = 0.993$) at various non-dimensional time: (a) $t = 10$; (b) $t = 40$; (c) $t = 60$ and (d) $t = 80$.

reduction in wake length as $Da$ as well as porosity is increased. The shifting of the separation point downstream contributes to this phenomenon.

In case of a solid cylinder the downstream separation occurs for $Re$ beyond 7. In contrast to the solid cylinder, the porous cylinder allows a finite amount of fluid to pass through with a non-zero velocity at the interface. With increasing $Da$ the velocity of the fluid at the interface increases. This velocity has the effect of reducing the relative importance of the inertial forces in the external field. Hence separation must be delayed. Fig. 8 shows the critical Reynolds number at which flow separation occurs as a function of $Da$. Flow separation occurs at $Re = 7$ for $10^{-6} \leqslant Da \leqslant 10^{-3}$. For this range of $Da$ the fluid velocity at the interface is negligible (of the order of $10^{-6}$). At $Da = 10^{-2}$ flow separation occurs for $Re > 10$. At a higher Darcy number of 0.02 separation is considerably delayed up to $Re = 17$. Hence, a pronounced delay in flow separation will occur for the case of a porous bluff body subjected to a transverse flow at higher $Da$.

The effect of the porous cylinder is to partially divert the flow. Some streamlines bypass the cylinder entirely, whereas others pass through a very small part. The streamlines at high permeability, i.e., large Darcy number is presented in Figs. 9a–e for $Re = 1$, 10, 20, 30 and 40. A large porosity corresponds to more void volume in the cylinder for fluid to flow through. The streamlines easily penetrate the porous region when Darcy number is high. A stream entering the porous cylinder cannot pass right through it, because of the recirculation set up by the external field at the rear end. Hence the streamline bypasses the wake. Both the main and the recirculating streams leaving the porous cylinder near the separation point have an effect very similar to injection from a porous surface into the main field. The streamline patterns at higher Reynolds number ($Re = 20$) show that the recirculation bubble forms at the downstream side of the cylinder. The center of the bubbles is slightly pushed away from the surface of the porous cylinder compared to the solid cylinder case.

The streamlines at lower values of Darcy number ($Da = 10^{-6}$) are presented in Figs. 10a–d for $Re = 10$, 20, 30 and 40. At this

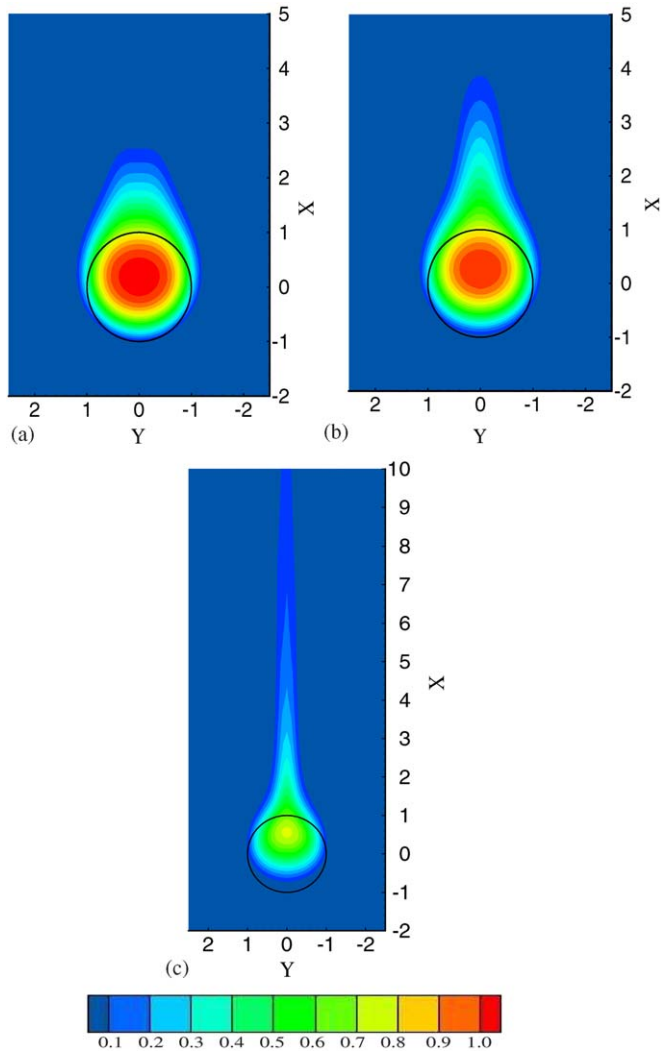


Fig. 14. Concentration field in and around the porous cylinder for $Re = 1$ and $Da = 10^{-2}$ ($\varepsilon = 0.993$) at various non-dimensional time (a) $t = 10$; (b) $t = 20$ and (c) $t = 50$.

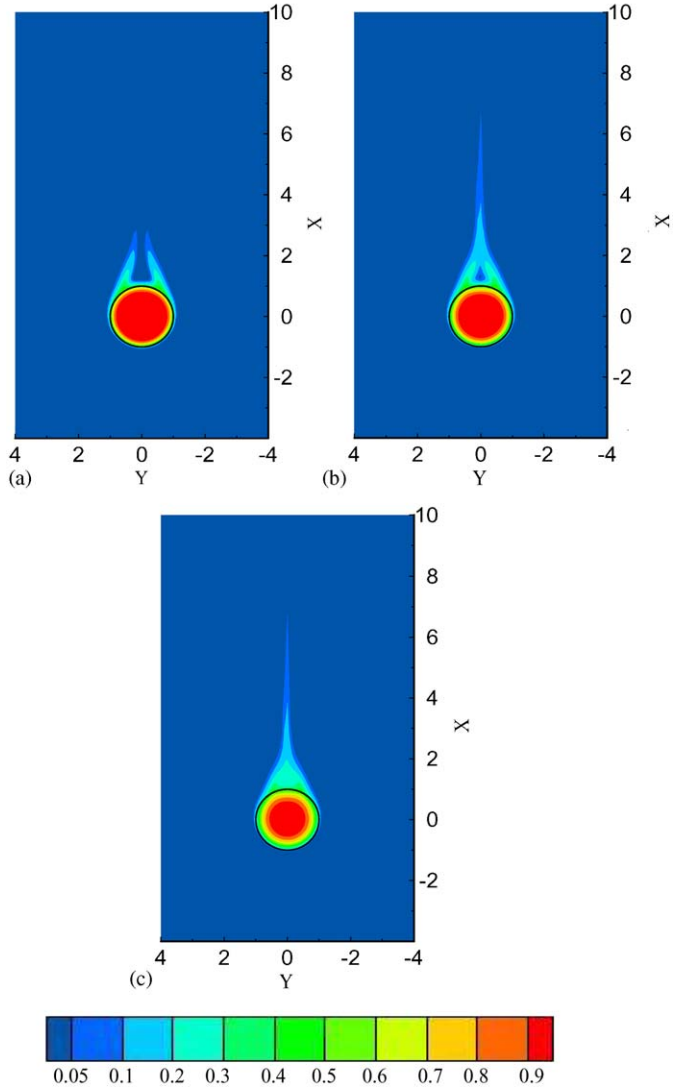


Fig. 15. Concentration field in and around the porous cylinder for $Re = 10$ and $Da = 10^{-6}$ ($\varepsilon = 0.629$) at a non-dimensional time: (a) $t = 50$; (b) $t = 100$ and (c) $t = 200$.

value of Darcy number the streamlines bypass the cylinder and the wake is similar to that of flow past a solid cylinder. The wake consists of two vortices attached to the downstream sides of the cylinder. The penetration through the cylinder is very small. The wake remains symmetric for the range of Reynolds number considered in this paper ($Re \leqslant 40$).

The vorticity contours are presented in Figs. 11a–e for $Re = 1, 10, 20, 30$ and 40 when $Da = 10^{-2}$ with dashed lines used for negative values and solid lines for positive ones. The wake is symmetric and two equal and opposite vortices are formed at the downstream side of the cylinder. The strength of the vortices are reduced in comparison with the solid cylinder case. For a solid cylinder, the vorticity diffuses from the surface into the external flow field, whereas, vorticity diffuses into both the external and internal flow fields when a porous cylinder is considered. Figs. 12a–d shows the vorticity contour at $Da = 10^{-6}$ for $Re = 10, 20, 30$ and 40. At this Darcy number, unlike $Da = 10^{-2}$ case, the vorticity fails to diffuse through the porous cylinder and the vorticity diffusion occurs only in the external flow field resembling that of a solid cylinder.

The temporal evolution of the concentration field around the porous cylinder for two cases of Darcy number $Da = 10^{-2}$ ($\varepsilon = 0.993$) at Reynolds number $Re = 20$ and 1 and $Da = 10^{-6}$ ($\varepsilon = 0.629$) at $Re = 10$ for a Schmidt number $Sc = 600$ are given in Figs. 13–15. Figs. 13a–d display the instantaneous distribution of concentration at $Da = 10^{-2}$ ($\varepsilon = 0.993$) and $Sc = 600$ at four different non-dimensional time $t = 10, 40, 60$ and 80. At time $t = 10$ the fluid is strong enough to ooze through the cylinder. Nearly 40% of the solute present in the porous region is washed away to the rear side due to strong convection of the fluid to form two symmetric plume structures in the downstream. The plumes are almost parallel to each other. The contour maps of instantaneous concentration field and vorticity have some similar features as both are being transported by the flow in the wake. At a non-dimensional time 40, the plumes meander the

recirculation region at the rear side of the cylinder and is about to attach together to form a single plume. The dimensionless concentration, $\phi$, now at the cylinder core is reduced to 0.9. The two symmetric plumes join together to form a single-tail-like structure at time, $t = 60$. In the context of marine sinking aggregates, this trail may be sensed by zooplankton, which attempt to follow the trail and colonize the particles. It can be seen that mixing of solute in the ambient fluid is slow in the recirculation region. The length of the tail is found to be 16 times the radii of the cylinder. At time 80, a long slender plume is formed at the downstream with decreasing concentration at the outer edge. The slender plume of high concentration persist for long duration in the wake of the aggregates. As described by Kiorboe et al. (2001), this plume have a significant effect on phytoplankton growth in the euphotic zone. The concentration is almost reduced to 0.4 at this time and the cylinder has almost lost all of its initial contents. The tail is found to grow in length with reduced concentration. The length of the tail now is about 20 times the cylinder radii and it is attached at the rear end.

The concentration field at a low Reynolds number $Re = 1$ at $Da = 10^{-2}$ for $Sc = 600$ is plotted in Figs. 14a–c. At this low $Re$ the mass transfer is mostly due to diffusion and a mixture in the upsteam side of the cylinder is evident from the figure. The mass transport phenomenon at this $Re$ is entirely different compared to higher $Re$ case. The rate of mass transfer from the porous cylinder is rather slow. Unlike the higher $Re$ case, the plume is thicker in size with a blunt edge.

The instantaneous concentration field for the case of cylinder with low Darcy number, $Da = 10^{-6}$ (i.e., $\varepsilon = 0.629$) is presented in Figs. 15a–c. We present the solution for $Re = 10$ and $Sc = 1000$, which produces the Peclet number 10,000 and compared it with the solution provided by Kiorboe et al. (2001) for the stokes flow past a solid sphere. Similar to the previously discussed case, i.e., $Da = 10^{-2}$ two non-parallel, symmetric plumes having a concentration of about 0.25 are formed at the downstream side of the cylinder. At time $t = 50$, the concentration is found to be maximum inside the porous region up to a radius of 0.95. At time 100, the symmetric plumes are found to attach together. A small region with almost zero concentration is formed near the rear stagnation point of the cylinder. This region is the flow recirculation region where no mixing of solute has taken place at this instant of time. The tail has a length of $6.9a$. The region of zero concentration at the rear end of the cylinder cease to exist at $t = 200$. At this instant the concentration is still high ($\phi = 1.0$) up to a radial distance of 0.75 from the center of the cylinder, and it decreases towards the outer edge. The tail length is found to be the same as that of the previous time of $t = 100$. The mixing and eventually the formation of the slender plume and the depletion of the concentration in this case is found to be much slower when compared to higher $Da$ case. The distribution of concentration at large time ($t \geqslant 100$) is "some what" similar to the stokes model for a solid sphere provided by Kiorboe et al. (2001). However, the length of tail of lower concentration in the wake is much smaller compared to the solution provided by Kiorboe et al. (2001). Our result shows that the long slender plume in the wake of the sinking aggregates persist for long duration.

## 5. Conclusion

A numerical study of the flow and concentration field in and around a permeable cylinder has been made through a single-domain approach. We found that the flow field remains steady for the range of Reynolds number considered (i.e., $1 \leqslant Re \leqslant 40$). The non-linear advection terms along with the Forchheimer term are found to be insignificant inside the porous region in the range of Reynolds number and Darcy number considered. The drag experienced by the porous cylinder reduces monotonically with the increase of $Re$ and decrease of $Da$. The reduction in $\overline{C}_D$ due to the increase of permeability is more pronounced in the lower range of Reynolds number, i.e., $Re \leqslant 5$. The angle of separation and wake length reduces as the Darcy number increases. The concentration field shows a plume which extends up to 20 times the radius of the cylinder when $Da = 10^{-2}$.

## Acknowledgment

One of the authors gratefully acknowledges the grant received from the Max Planck Institute for Marine Microbiology, Bremen, Germany.

## References

Adler, P.M., 1992. Porous Media: Geometry and Transports. Butterworth-Heinemann, Stoneham, MA.

Alldredge, A.L., Gotschalk, C., 1988. In situ settling behaviour of marine snow. Limnology and Oceanography 33, 339–351.

Alldredge, A.L., Gotschalk, C., 1989. Direct observations of the mass flocculation of diatom blooms: characteristics, settling velocity and formation of diatom aggregates. Deep Sea Research: Part A—Oceanographic Research Papers 36 (2), 159–171.

Basu, A.J., Khalili, A., 1999. Computation of flow through a fluid–sediment interface in a benthic chamber. Physics of Fluids 11 (6), 1395–1405.

Beckermann, C., Viskanta, R., 1988. Double diffusive convection during dendritic solidification of a binary mixture. Physicochemical Hydrodynamics 10, 195–213.

Braza, M., Chassaing, P., Minh, H.H., 1986. Numerical study and physical analysis of the pressure and velocity fields in the near wake of a circular cylinder. Journal of Fluid Mechanics 165, 79–130.

Dennis, S.C.R., Chang, G.Z., 1970. Numerical solutions for steady flow past a circular cylinder at Reynolds numbers up to 100. Journal of Fluid Mechanics 42 (3), 471–489.

Fornberg, B., 1980. A numerical study of steady viscous flow past a circular cylinder. Journal of Fluid Mechanics 98 (4), 819–855.

Heier, K., Von Wolfersdorf, L., 1990. Numerical evaluation of potential flow past a circular cylinder with porous surface. Zeitschrift fur Angewandte Mathematik und Mechanik 70, 65–66.

Jimenez-Islas, H., Lopez Isunza, F., Ochoa Tapia, J.A., 1999. Natural convection in a cylindrical porous cavity with internal heat source: a numerical study with Brinkman extended Darcy model. International Journal of Heat and Mass Transfer 42 (22), 4185–4195.

Kiorboe, T., Thygesen, U.H., 2001. Fluid motion and solute distribution around sinking aggregates, II: implications for remote detection by colonizing zooplankters. Marine Ecology Progress Series 211, 15–25.

Kiorboe, T., Ploug, H., Thygesen, U.H., 2001. Fluid motion and solute distribution around sinking aggregates, I: small-scale fluxes and heterogeneity of nutrients in the pelagic environment. Marine Ecology Progress Series 211, 1–13.

Masliyah, J.H., Polikar, M., 1980. Terminal velocity of porous spheres. Canadian Journal of Chemical Engineering 58, 299–302.

Mathelin, L., Bataille, F., Lallemand, A., 2002. The effect of uniform blowing on the flow past a circular cylinder. Journal of Fluids Engineering 124 (2), 452–464.

Nandakumar, K., Masliyah, J.H., 1982. Laminar flow past a permeable sphere. Canadian Journal of Chemical Engineering 60, 202–211.

Nield, A.D., Bejan, A., 1998. Convection in Porous Media. Springer, New York.

Nithiarasu, P., Seetharamu, K.N., Sundararajan, T., 1997. Natural convective heat transfer in a fluid saturated variable porosity medium. International Journal of Heat and Mass Transfer 40 (16), 3955–3967.

Noymer, P.D., Glicksman, L.R., Devendran, A., 1998. Drag on a permeable cylinder in steady flow at moderate Reynolds numbers. Chemical Engineering Science 53 (16), 2859–2869.

Patankar, S.V., 1980. Numerical Heat Transfer and Fluid Flow. Hemisphere Publishers, New York.

Somasundaram, P., Mysels, K.J., 1975. Steady-state flow in a porous cylinder with permeable walls and restricted or unrestricted ends. Journal of Fluids Engineering 97, 379–380.

Sucker, D., Brauer, H., 1975. Investigation of the flow around transverse cylinders. Wärme Stofübertragung 8, 149–158.

Vafai, K., Kim, S., 1989. Forced convection in a channel filled with porous medium: an exact solution. ASME Journal of Heat Transfer 111 (4), 1103–1106.

Vainshtein, P., Shapiro, M., Gutfinger, C., 2002. Creeping flow past and within a permeable spheroid. International Journal of Multiphase Flow 28 (12), 1945–1963.

Vainshtein, P., Shapiro, M., Gutfinger, C., 2004. Mobility of permeable aggregates: effects of shape and porosity. Journal of Aerosol Science 35 (3), 383–404.

Vanni, M., 2000. Creeping flow over spherical permeable aggregates. Chemical Engineering Science 55 (3), 685–698.

Von Wolfersdorf, L., 1988. Potential flow past a circular cylinder with porous surface. Zeitschrift fur Angewandte Mathematik und Mechanik 68, 11–19.

Von Wolfersdorf, L., Mönch, W., 2000. Potential flow past a porous circular cylinder. Zeitschrift fur Angewandte Mathematik und Mechanik 80, 457–471.